Available online at www.sciencedirect.com

ScienceDirect

Procedia Structural Integrity 37 (2022) 477–484

Structural Integrity Procedia

www.elsevier.com/locate/procedia

ICSI 2021 The 4th International Conference on Structural Integrity

Impact of mechano-sorptive loading on crack propagation of notched beams of White fir and Okume

Martian Asseko Ella[a],Giacomo Goli[c], Samuel Ikogou[b], Joseph Gril[a,e], Eric Fournely[a], Gaël Godi[a], Rostand Moutou Pitti[a,d]*

[a]*Clermont Auvergne Université, CNRS, Clermont Auvergne INP, Institut Pascal, F-63000 Clermont-Ferrand, France*
martian.asseko_ella@etu.uca.fr
[b]*USTM, Ecole Polytechnique de Masuku, BP 901 Franceville, Gabon*
[c]*University of Florence, DAGRI-Department of Agriculture, Food, Environment and Forestry, 50145 Firenze, Italia*
[d]*CENAREST, IRT, BP 14070, Libreville, Gabon*
[e]*Université Clermont Auvergne, INRA, PIAF, F-63000 Clermont Ferrand, France*

Abstract

The paper presents the experimental results of the crack process induced by viscoelastic effect and mechanical loadings. The notched specimens are White fir and Okume with dimensions equal to 160x12x60mm and notch length of 20mm. These specimens were tested in 3-point bending for 5 days under an initial stress of 80% of the rupture stress. At the end of these 5 days, we applied a second stress corresponding to 100% of the rupture stress. These tests were carried out under a sorption cycle of 45-75% relative humidity and at a constant temperature of 20°C. Monitoring of the crack propagation was performed by using an USB microscope. The results show that the crack propagation is accentuated by the drying effects on the one hand and by the effects of the applied stress on the other hand. The results show that crack propagation is influenced by viscoelastic effects, and by mechano-sorptive effects as shown in Figure 1. The crack propagation is more important when mechano-sorptive effects occur, especially during the drying.

Keywords: Energy release rate;Crack propagation; Mechano-sorptive creep;Viscoelastic creep;

*Rostand Moutou Pitti Tel. : +3306795A82425
rostand.moutou_pitti@uca.fr

10.1016/j.prostr.2022.01.112

1. Introduction

The current economic and environmental context is a major advantage for timber constructions, which are otherwise dominated by steel and concrete constructions. Unfortunately, in their long-term or short-term structural use, the interactions between mechanical and environmental stresses on these timber structures can strongly modify their mechanical behaviour. This makes their implementation more complex and can lead to a shortened service life. Although several studies have been carried out to understand and characterize the mechanical behaviour of wood in the long or short term under various mechanical stresses to date, such as the creep of wood in a variable environment Dubois *et al*. (2005) and Dubois *et al.* (2012). Very few studies exist yet on the simultaneous coupling of the effect of wood moisture content, crack parameters and viscoelastic and mechano-sorptive wood creep. The known work to date in this field [Hamdi et al. (2018)] studied the impact of the coupling of these 3 parameters on wood, particularly for creep tests in a variable environment or tension tests in a constant environment. Their work shows that there is a real impact of the interaction of these three parameters on wood by observing that humidification favoured the increase in wood strain and that the drying phase was conducive to the initiation and propagation of cracks [Pambou *et al*. (2019)]. However, it did not allow to better decouple the contribution of moisture content and mechanical effects on the crack process.

The objective of this work is therefore to study the influence of mechanosoptive and viscoelastic effects on wood crack to better understand the contribution of moisture content on wood crack. To this end, we carried out creep tests combined with fracture on Okume and White fir specimens under controlled relative humidity cycles and at a constant temperature of 20°C.

Nomenclature

MC	Moisture content
MC_Int	Moisture interpolated with measurements of shrinkage and swelling of the dimensional transducers
MC_Exp	Moisture calculated with the measurements of the successive weighings
Yc, Y_R, Y_T	Deflection of the transducers of the center and both sides
m_t	Mass at a time t (g)
m_0	Mass in anhydrous state (g)
a_0	Initial crack length (mm)
ε	Strain

2. Material and methods

2.1. Estimation of the loading forces

Before carrying out our creep tests, we first carried out static 3-point bending tests until the notched specimens broke. These tests allowed us to estimate the forces to be applied to the specimens during the tests. The specimens are of dimensions equal to 6x12x160mm. They were tested in 3-point bending and are oriented in the direction of the threads. The tests were performed on 6 specimens of each species. Tab.1 shows the average values and standard deviations of the rupture force, as well as the forces applied for the test. These forces correspond to 80% and 100% of the rupture force obtained.

Table 1. Rupture forces and loading forces of specimens

Species	Rupture force (daN)	80% Rupture force (daN)	100% Rupture force (daN)
Okume	16.75 (1.19)	13.4	16.75
White fir	13.69 (1.26)	10.95	13.69
() standard deviation			

2.2. Experimental set-up for viscoelastic and mechano-sorption tests coupled with crack

After determining the forces to be applied, we performed 3-points bending creep tests. The beams tested have the same geometrical configuration as those used for the static tests (Fig.1). Each beam is equipped with 3 transducers, two at the sides and one in the centre (Fig.1). The side transducers (T_L and T_R°) are used to estimate the shrinkage and swelling on the one hand and to correct the deflection at the centre on the other. The central transducer (T_C) is used to measure the displacement in the centre of the beam. At the two ends of the beams (A) and (B), we made notches of length (Lr) of 20mm and height (h_R) of 6mm corresponding to the half height of the beam.

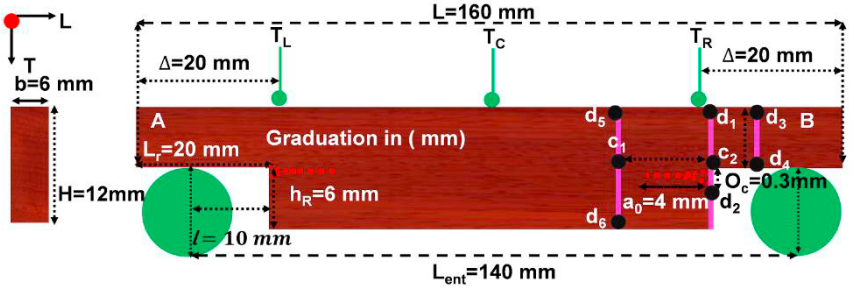

Fig. 1. Geometry of the tested beams.

We also initiated a crack length (a0) of 4mm and a crack opening (Oc) of 0.3mm with a cutter blade to facilitate crack propagation. The initial crack opening corresponds to the thickness of the cutter blade.

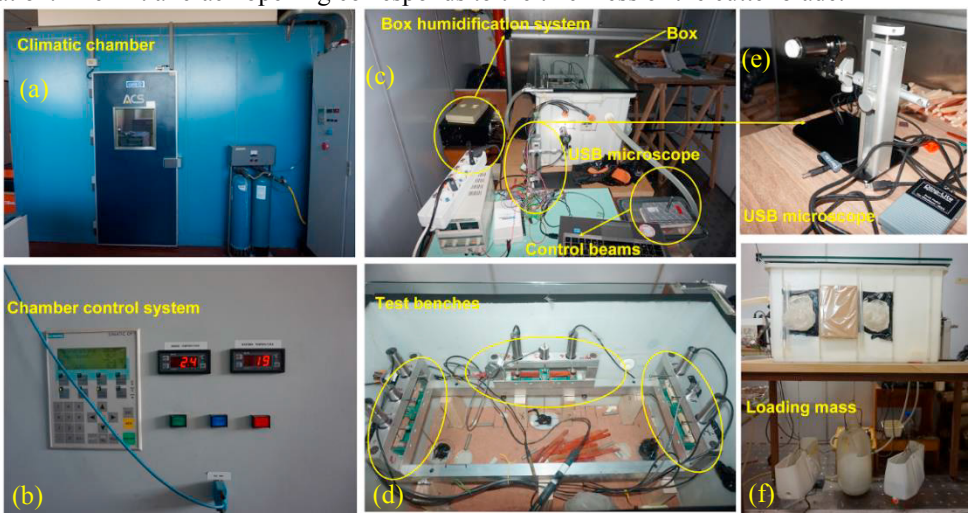

Fig. 2. (a) Climatic chamber; (b) chamber control system; (c) experiment set up ;(d) test benches; (e) USB microscope ;(f) loading for creep test.

The monitoring of the crack was performed from the outside of the box, as it was difficult to insert the microscope into the box without touching the tested beam. Each end of the beam was graduated in millimeters and marked by two vertical lines (d5d6) and (d1c2) 10 mm apart (c1c2). These two lines allowed us to calibrate horizontally the real dimensions of the image according to the magnification of the image that the microscope gives us. When taking a picture, these two vertical bars were filmed. The estimation of crack opening was done by measuring the variation of the distance (d1d2) close to the right of the notch, after having also calibrated vertically the image according to the real distance given here by the straight-line (d3d4) of initial distance equal to 6 mm.

The tests were carried out in a plastic box covered with a glass panel, placed in a climatic room (Fig.2a) where the temperature and relative humidity were kept constant at 75% and 20°C as shown by the external control system

(Fig.2b). The box (Fig.2c) was equipped with 3 mini 3-points bending benches with 3 transducers (Fig.2d). The box was humidity controlled by a humidity pump. The moisture content of the specimens was monitored by successive weighing of control specimens. The estimated moisture content was given by equation (1). These specimens were placed in a mini box connected to the experimental box by a pipe, allowing the taking of measurements without disturbing the tested specimens. The monitoring of crack parameters, crack length and crack opening, was done by taking images with an electronic USB microscope. The method for estimating these parameters and the operation of this microscope will be detailed in the following paragraph. At the bottom of the box, 3 holes were made under the test benches for loading the specimens. The test specimens were loaded in the wet state under constant stress corresponding to 80% of the stress at failure under a first hydric cycle of 45 to 75% relative humidity (RH). After this first cycle, if no crack was observed, additional loads were added to the initial loading to enhance the crack process and trigger beam failure. The added loading corresponded to a total load level of 100% of the estimated failure stress (Tab. 1). The additional loads were added every 30 minutes to avoid abrupt failure of the beam. After this overloading we continued with a second moisture cycle from 45 to 75% RH.

$$Mc(\%) = \frac{m_t - m_0}{m_0} \cdot 100 \tag{1}$$

2.3. Estimation of crack parameters: crack opening and propagation

The monitoring of the evolution of the crack parameters was done with a USB microscope. The crucial advantage of this device is that the image can be taken in any position and that one is not forced to keep it fixed. This microscope is equipped with a lens allowing to adjust the image size and magnification so that the image remains sharp. When taking a picture, the microscope automatically records the image number, date, time, image size and magnification. This information is very important for data processing.

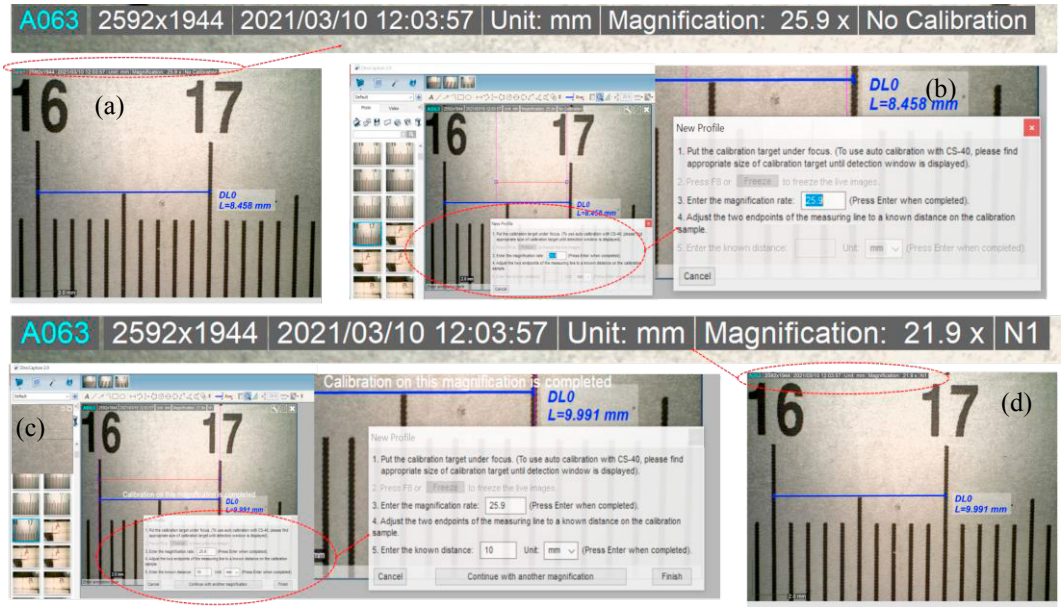

Fig. 3. Estimation of cracking parameters with the USB microscope (a) image without calibration; (b) calibration of magnification; (c) calibration of real distance; (d) calibrated image.

All this information is visible above the image in the circled area. The microscope is set by default in the no calibration mode and this mode is not very accurate and does not describe the real dimensions of the image (Fig. 3a).

To solve this difficulty, we calibrated the size of each image according to the real distance and its magnification (Fig. 3b) and (Fig. 3c). In Fig. 3d an example of crack length estimation is shown. This operation is done in 4 steps. The first one consists in taking a sharp image with the microscope on which we have two reference points of known distance (Fig. 3a), in our case we took an example with a ruler graduated on an interval d 16 and 17 cm. When estimating the distance of this image, we notice that the distance reading is wrong because the real dimensions of the image have not yet been calibrated. By calibrating the image with the magnification (25.9) and a known real distance of the image (10 mm) we get a less erroneous reading of the measured distance (Fig. 3d). On the final image we can see that the measured distance is not the same as the known distance. The error is of the order of 0.09%, which is negligible and can be justified by the difference in precision of our measuring tools, in particular the graduated ruler precise to the millimeter, unlike the microscope which is very precise.

3. Result et discussion

3.1. Effects of mechano-sorptive viscoelastic behaviour on crack propagation

First we show the strain due to the mechano-sorptive and viscoelastic behaviour effect on the crack propagation of the tested beams until the rupture of the test 1 (Fig.4) and the test 2 (Fig.5). Only Okume (Fig.5a) did not fail during the first two sorption cycles. In parallel for each test, we will present the evolution of the experimentally measured moisture content (MC_Exp) and the one we estimated (MC_Int) as shown in (Fig.4d) and (Fig.4e) for test 1 and (Fig.5c) and (Fig.5d) for test 2. The estimation of the moisture content was done by correlating the experimental moisture content measurements with the effects of shrinkage and swelling measured by the T_R and T_L sensors. A very good correlation between these two measurements can be seen. Thus, these figures show the propagation of the crack increment under the effects of viscoelastic and mechano-soprtive strain of Okume and White fir specimens during the first cycle and the beginning of the second sorption cycle. A sorption cycle takes place over 6 days, including a humidification phase at 75% RH of one day, a drying phase at 45% RH of 3 days and a re-humidification phase at 75% RH of 4 days on the 4th day. At the end of the third day of rehumidification, we add additional loads and start the second sorption cycle. The viscoelastic and mechano-sorptive strain were estimated by the following equation:

$$\varepsilon = \frac{2 \cdot 3 \cdot H}{1 + 7 \cdot \lambda^3} \frac{y_c - y_{RL}}{L_{ent}^2} \tag{2}$$

with $\lambda = 2.l/L_{\text{ent}}$. $\lambda = 2 \cdot l / L_{ent}$

y_{RL} is the average of the deflections measured by the transducers on the T_R and T_L sides and the deflection at the centre measured by the T_C transducer. From these curves we can see that the instantaneous strain of Okume is greater than those of White fir. This is justified by their longitudinal modulus of elasticity, that of White fir being greater than that of Okume and therefore less rigid than White fir.

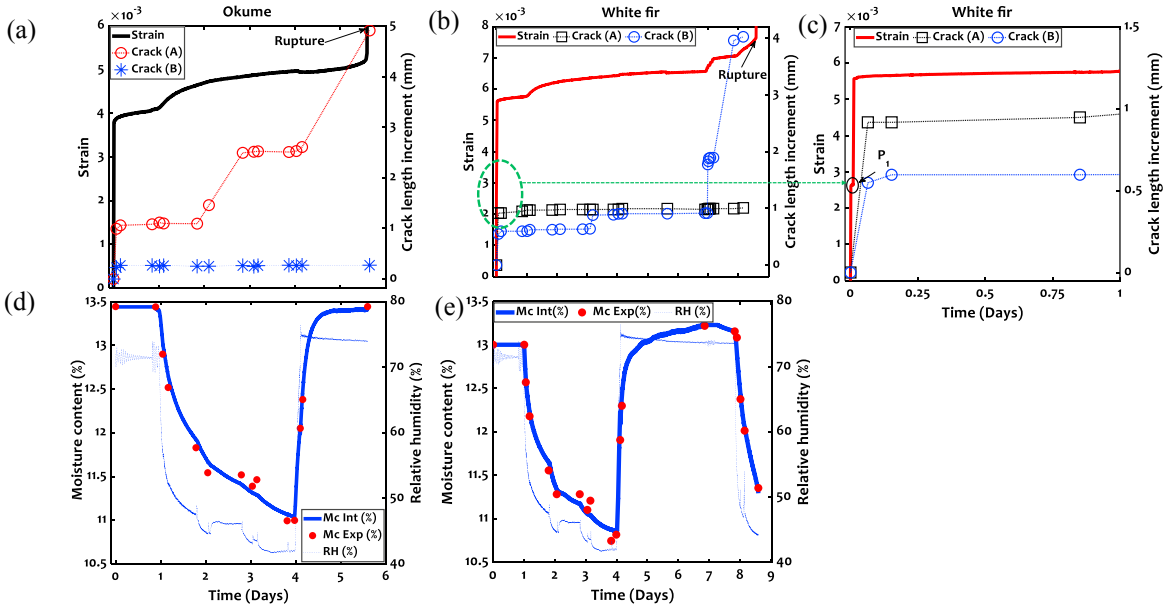

Fig. 4. Strain test 1(a) Okume; (b) White fir; (c) Okume; (d) White fir (e) Zoom White fir.

We zoomed in on the (Fig.4c) of White fir Test 1 during the instantaneous loading to better see the timing of the loading as shown by the circled area (P1). Apart from the effect of the loading, the instantaneous strain was enhanced by the crack and equals ($2.6x10^{-3}$). In these figures it can also be seen that the instantaneous loading of the beams leads in most cases to crack initiation.

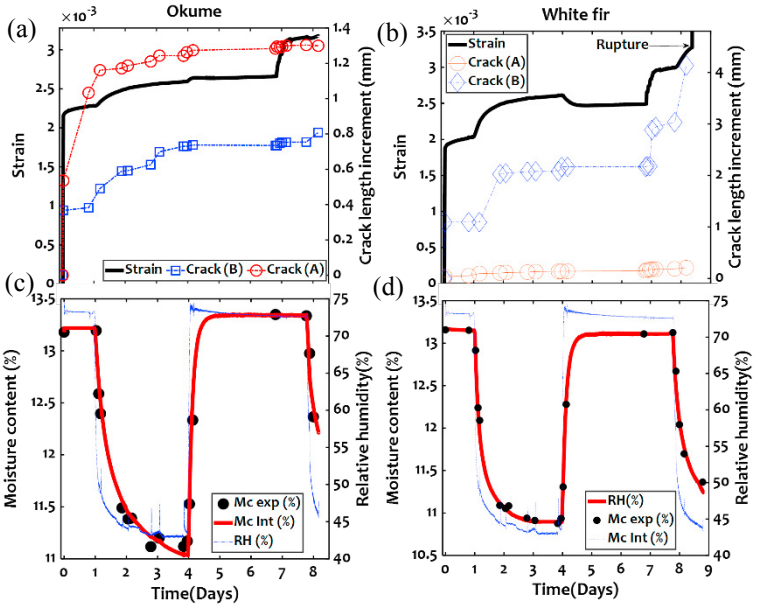

Fig. 5. Strain test 2 (a) Okume; (b) White fir; (c) Okume; (d) White fir.

The crack propagation tends to develop on one side of the beam while it remains almost constant on the opposite side, this is the case in (Fig.4a), (Fig.4c) and (Fig.5b). After loading the wood shows a viscoelastic behaviour. During

this phase the crack increment remains almost constant, but after the first drying the wood shows a mechano-sorptive behaviour and the crack increment tends to increase until the rupture of the beam. In the White fir test the rupture occurred during the drying phase, while in the Okume test it occurred during the wetting phase. This rupture during the humidification phase can be explained mainly by the effects of mechanical loading. In general, it appears that drying favours crack propagation in contrast to humidification where there is no crack. This observation confirms the results of Pambou *et al*. (2019) and Phan *et al*. (2016). During the second humidification on day 4, two types of phenomena are observed, namely pseudo-creep and pseudo-recovery, explained according to Hunt (1999) by a modified moisture expansion under the effect of the longitudinal deformation.

3.2. Effect of moisture content variations on crack openings

In this section we present the effect of the sorption cycle on the crack openings. Fig. 6 shows the behaviour of the crack openings under the effect of the variations of the experimental moisture content (Mc_exp) of the two faces A and B of the Okume (Fig. 6a) and (Fig. 6b) and White fir (Fig. 6c) and (Fig. 6d) specimens for test 1 and test 2. The crack openings increase during the drying phases; however, they remain constant during or close during the wetting phase. The increase in crack openings during the humification phase on day 7 is explained by the addition of additional loads from. The similar results observed by Pambou Nziengui *et al.*(2019) .

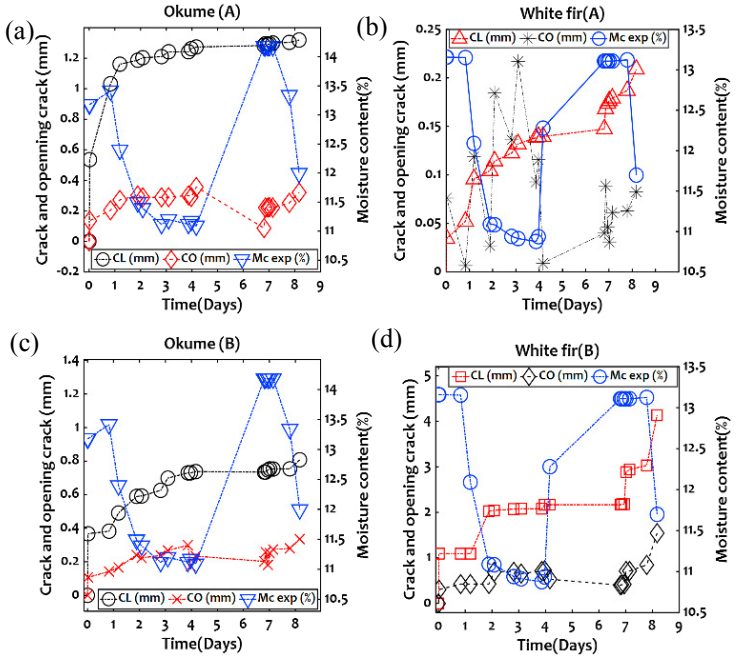

Fig. 6. Impact of moisture content variations on crack openings (a) Okume test 1; (b) White fir test 1; (c) Okume test2; (d) White fir test 2.

3.3. Energy restitution rate

In a second plane we present the evolution of the energy restitution rate in mode I as a function of the crack increment of the specimens of test 2. This energy restitution rate was calculated by the compliance method equation (3).

$$G = \frac{F_{ci}^2}{2 \cdot b} \frac{\Delta C}{\Delta a} \tag{3}$$

Avec $\Delta C = U_{ci} / F_{ci}$, U_{ci} is the crack opening generated by the critical force F_{ci}. In our case F_{ci} is constant during a cycle. Fig. 7 shows the evolution of the energy restitution rate as a function of the crack increment for Okume (Fig. 7a) and White Fir (Fig. 7b) from test2. The amount of initial energy required for crack propagation in Okume is slightly higher than that provided by White fir. Their values are respectively equal to 3.25 N.mm^{-1} and 2.5 N.mm^{-1}. This can be justified by the density of the two specimens tested which are 0.42 for the Okume beam and 0.41 for the White fir. This constant seems to confirm the observation of Odounga *et al*. (2019) on the effect of density on the rate of energy restitution where he noted that the rate of energy restitution of dense species was higher than that of less dense species.

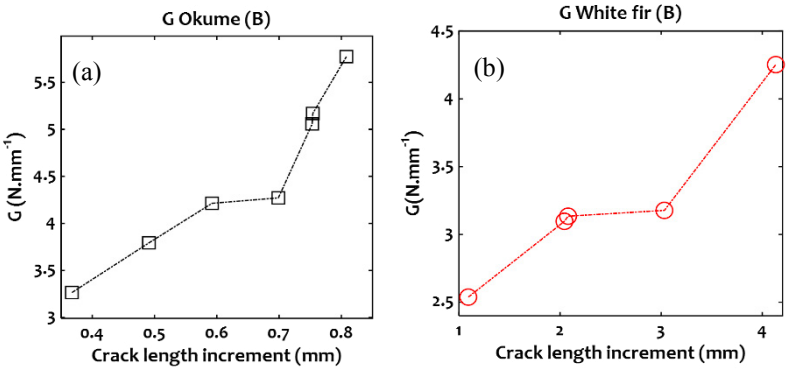

Fig. 7. Energy restitution rate for test 2 (a) Okume; (b) White fir

4. Conclusion and perspectives

This paper presents the study of the effects of mechano-sorptive and viscoelastic creep on wood crack. The study is done on notched specimens of White fir and Okume. These specimens were tested in the wet state and initially loaded to 80% of the rupture force for 6 days under a sorption cycle of (45% and 75% RH) before being loaded to 100% of the rupture force in a second stage. The monitoring of the crack parameters was done with a USB microscope. The results show that the mechano-sorptive effects accentuate the propagation of cracks and that the coupling of the two effects, namely crack and the mechano-sorptive effect, accelerates the strain of the wood until it breaks. Regarding the effect of drying on crack propagation, our observations agree with those of the literature. On the effect of drying on strain, we have however noticed that drying accentuates strain in the case of a mechano-symmetric creep test, contrary to a creep test in an uncontrolled environment where the effect of drying on strain is reversed.

References

Dubois, F. *et al.* (2012) 'Modeling of the viscoelastic mechano-sorptive behavior in wood', *Mechanics of Time-Dependent Materials*, 16(4), pp. 439–460. doi: 10.1007/s11043-012-9171-3.

Dubois, F., Randriambololona, H. and Petit, C. (2005) 'Creep in wood under variable climate conditions: Numerical modeling and experimental validation', *Mechanics of Time-Dependent Materials*, 9(2–3), pp. 173–202. doi: 10.1007/s11043-005-1083-z.

Hamdi, S. E., Piti, R. M. and Gril, J. (2018) 'Moisture driven damage growth in wood material: 3D image analysis for viscoelastic numerical model validation', *WCTE 2018 - World Conference on Timber Engineering*.

Hunt, D. G. (1999) 'A unified approach to creep of wood', *Proceedings of the Royal Society A: Mathematical, Physical and Engineering Sciences*, 455(1991), pp. 4077–4095. doi: 10.1098/rspa.1999.0491.

Odounga, B. *et al.* (2019) 'Mixed mode fracture of some tropical species with the grid method', *Engineering Fracture Mechanics*. Elsevier, 214(May), pp. 578–589. doi: 10.1016/j.engfracmech.2019.04.018.

Pambou Nziengui, C. F. *et al.* (2019) 'Notched-beam creep of Douglas fir and white fir in outdoor conditions: Experimental study', *Construction and Building Materials*. Elsevier Ltd, 196, pp. 659–671. doi: 10.1016/j.conbuildmat.2018.11.139.

Phan, N. A. (2016) 'Simulation of time-dependent crack propagation in a quasi- brittle material under relative humidity variations based on cohesive zone approach : application to wood'.